



## RESEARCH LETTER

10.1002/2013GL058913

## Key Points:

- Shearing reduces the initial surface roughness at all measurement scales
- Initial to final roughness ratio increases as a function of the slip distance
- The roughness ratio for a test is wavelength independent from above a few millimeters of displacement

## Correspondence to:

A. Sagy,  
asagy@gsi.gov.il

## Citation:

Davidesko, G., A. Sagy, and Y. H. Hatzor (2014), Evolution of slip surface roughness through shear, *Geophys. Res. Lett.*, *41*, 1492–1498, doi:10.1002/2013GL058913.

Received 1 DEC 2013

Accepted 6 FEB 2014

Accepted article online 10 FEB 2014

Published online 10 MAR 2014

## Evolution of slip surface roughness through shear

Guy Davidesko<sup>1,2</sup>, Amir Sagy<sup>1</sup>, and Yossef H. Hatzor<sup>2</sup>

<sup>1</sup>Geological Survey of Israel, Jerusalem, Israel, <sup>2</sup>Department of Geological and Environmental Sciences, Ben-Gurion University of the Negev, Beer Sheva, Israel

**Abstract** A significant part of displacement in fault zones occurs along discrete shear surfaces. The evolution of fault surface topography is studied here in direct shear laboratory experiments. Matching tensile fracture surfaces were sheared under imposed constant normal stress and sliding velocity. The roughness evolution was analyzed using measurements of surface topography before and after slip. We show that shearing reduces the initial surface roughness at all measurement scales. At all wavelengths, the roughness ratio between initial and final roughness increases as a function of the slip distance. For a given test, the roughness ratio increases with wavelength up to a few millimeters, beyond which the ratio becomes wavelength independent. At this region the roughness measured after slip follows a power law similar to that of the initial tensile fracture surface. We interpret this geometrical evolution as a consequence of the deformation stage of interlocked asperities which is followed by shear-induced dilation.

## 1. Introduction

Fault topography is one of the major determinants of slip distribution in earthquakes [Parsons, 2008]. It strongly affects resistance to shear [Wang and Scholz, 1994], critical slip distance [Ohanaka, 2004], fault dynamics [Dunham et al., 2011], fault gouge generation [Power et al., 1988], and near-fault stress fields [Dieterich and Smith, 2009; Griffith et al., 2010]. The process of shear-induced wear accumulation in rock discontinuities has been studied extensively both theoretically and experimentally [e.g., Power et al., 1988; Wang and Scholz, 1994; Boneh et al., 2013]. The direct effects of slip distance and wear generation on the geometrical evolution of fault surfaces have not been investigated as extensively, however, despite the great significance of these issues for proper understanding and modeling of natural faults evolution [Wang and Scholz, 1994; Renard et al., 2012]. Field measurements of fault surface geometry demonstrated that fault surfaces are rough at all measurable scales and lead to the suggestion that a universal power law characterizes fault surface roughness across a large range of scales, from submillimeters to ~ hundred meters [e.g., Power et al., 1988; Renard et al., 2006; Candela et al., 2009; Bistacchi et al., 2011]. Results of recent field measurements suggest an evolution of fault surface roughness with slip. Surfaces of relatively large-slip faults are statistically smoother than those of small-slip faults, when comparing geometrical sections at the same wavelength along the slip orientation [Sagy et al., 2007; Sagy and Brodsky, 2009; Bistacchi et al., 2011]. Quantifying the observed slip surface roughness evolution on the basis of field observations is, however, difficult because of the inherent variability in lithology and tectonic setting of the studied outcrops which affect wear. Furthermore, processes of postfaulting cementation and erosion can affect any exposed surface in the field and might conceal the actual fault surface morphology [Brodsky et al., 2011]. It is therefore unclear if the observed roughness characteristics in the field are uniquely related to friction and shear and how the measured surface roughness evolves as a function of slip distance at different scales. To resolve this ambiguity we performed laboratory measurement to characterize the evolution of slip surface topography as a function of shear using servo-controlled direct shear experiments (Figure 1a), coupled with accurate optical profilometer measurements (Figure 1b).

## 2. Experimental Approach

Roughness measurements of mesoscale surfaces were used historically primarily to evaluate scale-dependent shear strength of natural rock joints (up to 10 cm in length) [e.g., Rengers, 1970; Goodman and Dubois, 1972; Barton, 1973]. Later, the geometrical characteristics of shear fractures and their relationship to the applied loading history and slip distance were studied as models for natural faulting [Chen and Spetzler, 1993; Amitrano and Schmittbuhl, 2002]. Recently, Renard et al. [2012] documented slickenside development and roughness

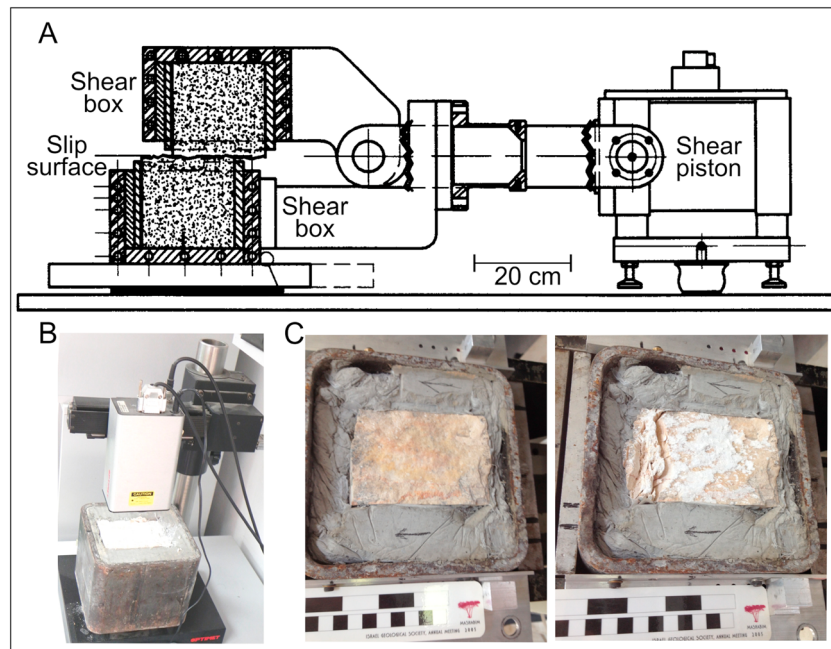


**Figure 1.** Experimental procedure: (a) The direct shear test assembly, (b) the optical profilometer, and (c) an example of a fractured limestone interface before and after direct shear testing. Note concentrated damage at asperity contacts. Upper scale is in inches; lower scale is in centimeters.

variations during slip of initially smoothed Halite samples. Here we focus on the effects of slip distance on shear surface geometry under steady state sliding condition. We first fracture a single prismatic rock block in tension mode using the three-point bending testing methodology and scan the fracture surface topography. Then, we shear the obtained tensile fracture surfaces in direct shear, ensuring the original fracture surfaces are in a perfectly matching configuration at the beginning of the shear test. Shearing is conducted under constant normal stress of 2 MPa and constant displacement rate of 0.05 mm/s using two closed-loop servo controlled hydraulic pistons, one for the normal (vertical in our test configuration) and the other for the shear (horizontal) loads (Figure 1a). Following the shearing, the fracture surface is scanned again, and the geometrical evolution, in term of roughness, is then analyzed.

We chose this alternative experimental approach because (1) by first inducing a tensile fracture, we generate a rough surface with topography comparable to the rough topography of natural fractures (Figure 1c); (2) the obtained initial surface roughness is not influenced by any artificial machining operations such as saw cutting or polishing; (3) by adopting this experimental procedure, the surface morphology can be measured before and after shear displacement, and the variations in the roughness profile can be examined between different shear distances and at different scales; and (4) fractures in nature are usually tight and/or partly cemented [e.g., *Power and Tullis*, 1989; *Muhuri et al.*, 2003], and many shear fractures in the Earth's crust indeed originated from initially tensile fractures [Segall and Pollard, 1983]. Therefore, the initially matching surfaces of the tensile fractures created in the lab better simulate natural fractures when compared to artificial or natural surfaces that are placed arbitrarily one against the other before shear testing is ensued.

The sample length parallel to the sliding direction is typically 15 cm, and the width normal to the sliding direction is typically 8 cm. We focus here on the geometrical modification of a fault surface in response to displacement range of 5 to 15 mm. Therefore, the ratio between the target displacement and surface length (0.03 to 0.1) falls well within the range measured for natural faults [see *Cowie and Scholtz*, 1992]. We used fine-grained limestone as a starting material with an average grain size of 300  $\mu\text{m}$ . Analysis of thin sections shows that internal pores are scarce with diameter typically much smaller than the mean grain size. The small grain size has been chosen in order to ensure that the characteristic grain dimension is smaller than the minimum slip distance during a single test. Note, however, that the chosen experimental configuration does not fully

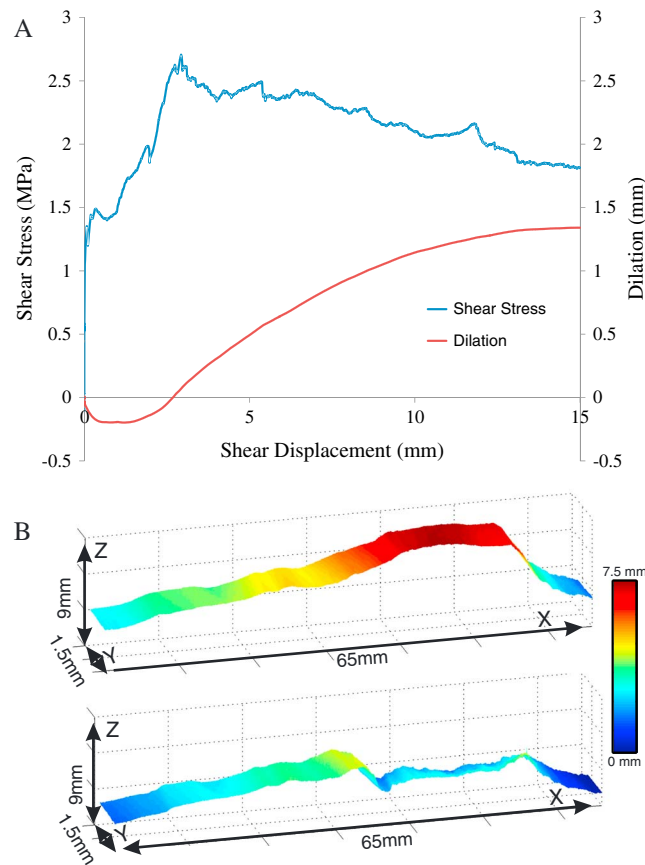


**Figure 2.** (a) Evolution of shear stresses and dilatation in a sample which was sheared to 15 mm under a constant normal stress of 2.0 MPa. Peak and residual shear strengths are readily identified as is characteristic of initially rough surfaces that are sheared under relatively low normal stress. Dilatation (positive in Figure 2a, along Z axis in Figure 2b) begins after ~2.5 mm of displacement and continues throughout the shear segment. A similar behavior is observed in all tested interfaces. (b) Topography scans of a slice of the sample include 50 adjacent profiles before (top) and after (bottom) slip. Note decrease in topographical amplitude after slip. Slip direction is along the X axis; topography is measured along Z axis.

the test (Figure 2a). The dilational response clearly indicates that during shear under the applied normal stress and with the given mechanical properties of the interface material, the overriding block tends to glide over the initial asperities, rather than completely shear through them, as typically observed in direct shear tests of rough rock joints [e.g., Goodman and Dubois, 1972]

We now examine the geometrical evolution of the tested surfaces as a function of slip. Surface topography was measured prior to and after shear using a laser profilometer (see Figure 2b). Every scan generated 640 parallel profiles with spacing of 0.1 mm ( $\Delta X$ ) parallel to the slip direction and 0.03 mm ( $\Delta Y$ ) perpendicular to the slip orientation, covering a total scanned area of approximately 1500 mm<sup>2</sup>. The roughness was calculated from the topography (Z axis); the resolution of the present device allows a reliable roughness analysis from wavelength above ~0.5 mm in the slip direction.

The results presented graphically in Figure 2b imply that for a given slip distance, the topography amplitude clearly decreases after slip. The particular example shown in Figure 2b was sheared to a distance of 15 mm, and it seems that the entire surface exhibits topographic degradation, yet we note that several other patches of the original surface were less affected.

As a sample topography scan typically contains about half a million points, reliable average values of roughness along the measured length scale can be obtained. The surface roughness is determined first by

represent natural faulting conditions at seismogenic depths, primarily due to the absence of confining pressure and induced pore pressure.

### 3. Results

Our results are based on five direct shear tests, each performed under a different prespecified displacement target. The initial surfaces were rather rough, with typical roughness amplitude of up to a few millimeters (see Figure 2b). As mentioned earlier, the tested surfaces were placed in a perfectly matching configuration before direct shear testing began. Most of the wear particles remained between the tested surfaces because the shear distance targets of 5 to 15 mm were relatively small compared to the much larger sample width of 80 mm. A representative direct shear test result is shown in Figure 2a where both shear stress and dilatation are presented as a function of shear displacement. In the tested configuration peak shear stress is typically attained after a shear displacement of ~2–3 mm, beyond which lower shear stress is required to continue shearing at the preset displacement rate of 0.05 mm/s, as typically observed when shearing rough joints. Following some initial compression, the interface begins to dilate in response to shear, through peak shear stress and until the end of

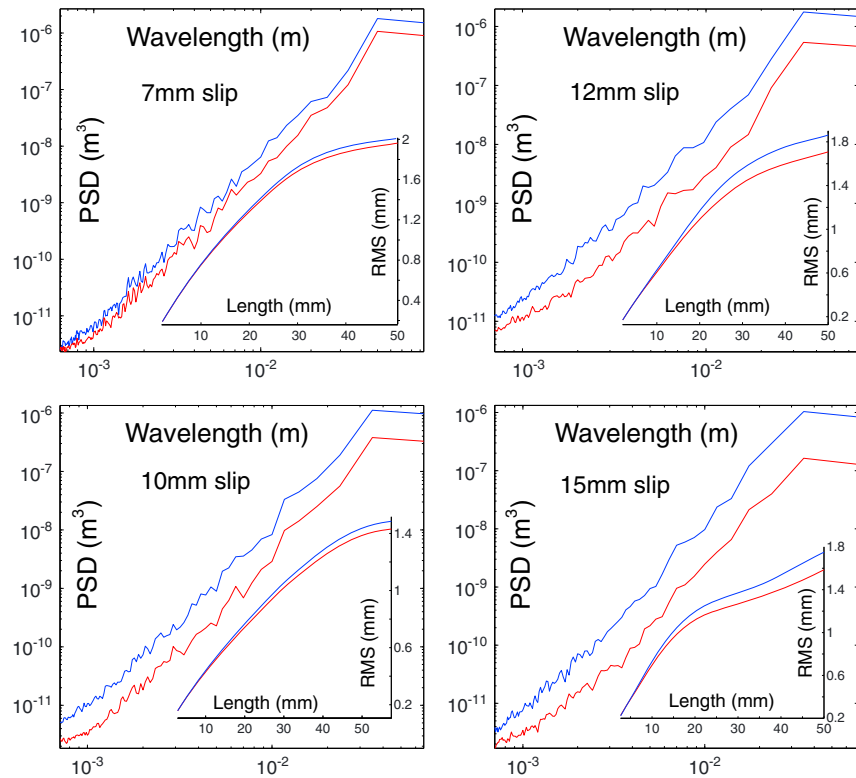


**Figure 3.** Surface roughness parallel to the slip direction before (blue) and after (red) slip for four different samples. Power spectral density (PSD) is presented on logarithmic scale, and RMS values are plotted on linear graph. Roughness decrease is observed for all tests along the entire measured lengths.

using the root-mean-square (RMS) roughness which is the average deviation of the topography from a planar line [Power *et al.*, 1988]. The RMS values are calculated for all scanned profiles in a given sample using increasing window lengths from 0.5 mm to 50 cm and are presented as a function of the profile section length (insets in Figure 3). We then use the power spectral density (PSD) which quantifies the strength of the sinusoidal components of the topography over a range of wavelengths ( $\lambda$ ) by performing Fourier decomposition [Brown and Scholz, 1985; Brodsky *et al.*, 2011].

A graphical summary of our results is presented in Figure 3 which demonstrates the roughness evolution for four different surfaces tested with increasing total slip distance, from 7 mm to 15 mm of slip. The figures present the measured roughness in the sheared samples by means of the RMS and PSD values as function of the section length and wavelength, respectively. We find that the measured roughness decreases as function of slip distance in all samples and for all measured scales. The RMS plots indicate that for all samples, the roughness increases nonlinearly with profile length with no observable large-scale cutoff, similar to natural surfaces [e.g., Power *et al.*, 1988; Candela *et al.*, 2009]. Yet one of the most interesting observations in our experiments is that the RMS difference (RMS of the initial surface for a given length-RMS of the final surface for the same length) also increases with increasing profile length in all of the experiments (Figure 3).

The PSD plots presented on logarithmic scales in Figure 3 demonstrate a relatively linear increase of the roughness as a function of wavelength. Moreover, it is shown that the difference between the roughness before and after slip increases as a function of slip distance but is relatively constant in each test. To better illustrate this new experimental finding, we present the roughness ratio (initial  $PSD_{(\lambda)}$ /final  $PSD_{(\lambda)}$ ) for any given run on the same plot (Figure 4a).

The figure shows that the roughness ratio in all tests can be roughly divided into two scale-dependent regions: up to a wavelength of a few millimeters the ratio increases with increasing wavelength, and then at the range of a few millimeters to a few centimeters the ratio remains relatively constant with increasing wavelength, but its value increases with the amount of slip (Figure 4b).

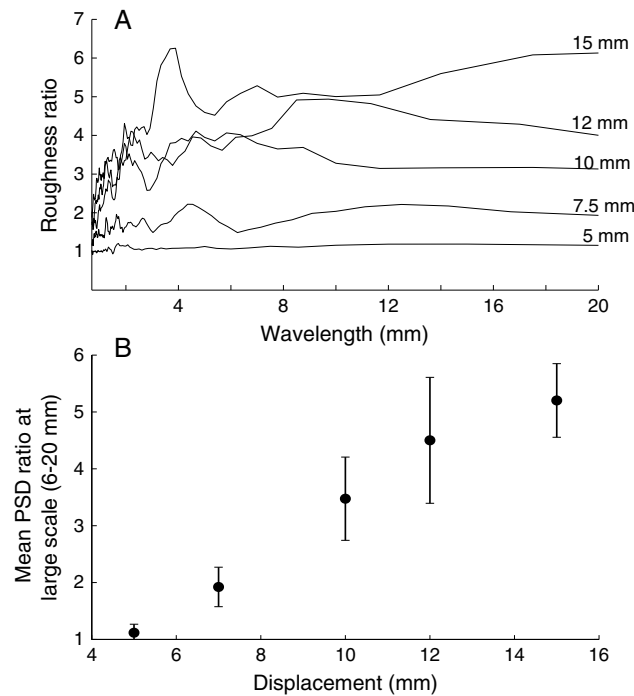


**Figure 4.** Roughness evolution during shear. (a) The roughness ratio (see text) for the five sheared surfaces along the measured range of length scales. The ratio value for all tests increases with wavelength up to ~5 mm and then becomes relatively constant. (b) The mean value of the PSD ratio at the 6–20 mm length scale (where the slope of the curves in Figure 4a is much more moderate) increases with slip.

asperities controls the magnitude of slip up to about ~3 mm of displacement where maximum shear resistance is mobilized. Beyond that point slip is controlled by the frictional resistance of the tested interface.

At wavelength below ~5 mm the roughness ratio values decrease with wavelength (Figure 4a), thus providing evidence for reduction of wear effectiveness for small-scale asperities. We explain this difference by the pronounced dilatational behavior of the tested interfaces in our experiments (Figure 2a). As shear displacement begins, the developed shear stresses concentrate at the contact points between the asperities on both surfaces. Plastic displacement beyond the elastic deformation of the asperity material (elsewhere referred to as “steady state sliding”) may ensue only when some of the asperity material fails, either by crushing or by shear. It is abundantly evident from the observed dilatational response (Figure 2a) that not all of the asperities are completely smoothed during sliding. We propose here that with increasing shear displacement, the relatively larger asperities are more likely, statistically, to interact with one another and to be smoothed by a certain amount, while the smaller asperities are expected to be less affected during the dilatational stage. It follows, therefore, that new space will be generated during sliding preferentially between asperities of smaller amplitude, and therefore these asperities will be less likely to interact during shear.

#### 4. Discussion

Although our range of measurements is not large enough for robust fractal analysis, the parallel linear PSD slopes that have been observed in our experiments (Figure 3) suggest that the PSD for lengths above few millimeters might be described by a power law with a relatively sharp power of 2.7–2.95, and consequently,

$$PSD = C_{(d)}\lambda^\beta, \text{ for } \lambda > 5 \text{ mm.} \quad (2)$$

where  $\beta$  is the slope of the PSD lines in Figure 3, and  $C_{(d)}$  is the slip dependent efficiency of the smoothing process. It is reasonable to assume that the coefficient of the power  $C$  which varies with slip distance also depends on slip dynamics, normal stress, and material properties. We interpreted the evolution of roughness expressed by equations (1) and (2), as a consequence of breaking of interlocked asperities [e.g., Scholz, 2002], yet

The observed results suggest that if  $F$  and  $G$  are two functions which define, respectively, the initial and the final PSD values as a function of wavelength then

$$F_{(\lambda)} = C_{(d)}G_{(\lambda)}, \text{ for } \lambda > 5 \text{ mm} \quad (1)$$

where  $C$  is a constant which depends on the amount of displacement ( $d$ ) in each shearing cycle.

Such a result is expected to be a product of shear deformation when all scales are affected and yield by shear deformation. In our case, because the surfaces are initially rough and well matched, fracture of interlocked asperities [Scholz, 2002] is probably the main mechanism for smoothing and localization. Yet at the small-scale range, the roughness ratio decreases suggesting that small geometrical fluctuations are less affected by shear-induced polishing. Figure 4 also demonstrates that detectable geometrical variations, or permanent surface damage (roughness ratio > 1), appear only after ~5 mm of displacement took place. This observation is consistent with the direct shear test result shown in Figure 2a which implies that elastic strain of the

it should be pointed out that this breaking does not smooth the surfaces spontaneously or completely and that the dilational behavior reduces the efficiency of the process at the relatively smaller scales. The dilational effect may be expected to be restrained with increasing normal stress, an issue we are currently investigating.

Let us now examine the relevance of our observations to natural fault roughness evolution during shear. Wear of solid materials is usually characterized by a stage of transient wear accumulation at a high rate, followed by a stage of steady state wear accumulation at a low rate [Archard, 1953; Queener *et al.*, 1965]. While both stages are dependent upon the slip amount and normal stress, it was shown that the transient stage is strongly controlled by the initial roughness of the tested interface [Queener *et al.*, 1965; Wang and Scholz, 1994]. Power *et al.* [1988] suggested that wear in natural faulting is always transient, because they assumed that faults are rough at all scales and argued that the amount of slip is relatively small comparing to the fault length. Although we did not measure wear volume, our experiments which involved relatively small slip amounts on rough surfaces are reasonably well within this transient stage (Figure 4b).

If equation (2) remains valid at larger scales, then it may represent a good approximation for the roughness evolution law of natural faults during slip, and the surface roughness may be considered as self affine [Feder, 1988; Amitrano and Schmittbuhl, 2002]. In such surfaces, if the horizontal direction  $x$  is viewed at magnification  $\lambda$ , the vertical direction  $z$  must be magnified by  $\lambda^H$ , (where  $H$  is the Hurst exponent which relates to the PSD slope  $\beta$  via  $H = (\beta - 1)/2$ ), in order to maintain scale invariance, [Power *et al.*, 1988; Brodsky *et al.*, 2011]. However, the relatively high Hurst exponent values obtained here (0.85–0.97) are closer to typical roughness exponent values of  $\sim 0.8$  characteristic of tensile and shear fractures [e.g., Bouchaud *et al.*, 1990; Amitrano and Schmittbuhl, 2002] rather than the more moderated Hurst exponents of  $\sim 0.6$  found parallel to the slip direction in mature fault surfaces [Renard *et al.*, 2006; Candela *et al.*, 2009]. It is possible therefore that our PSD slopes are typical to wavelengths which are large comparing to the slip amount along a sheared surface.

When the measured PSD slope of the sheared surface is less sharp than the slope of the initial surface, as observed here for wavelength below  $\sim 5$  mm, reduced effectiveness of smoothing with decreasing wavelength is suggested. In our experiments, dilation, as discussed above, can explain the reduced effectiveness of smoothing at the smaller scales. During natural faulting, however, internal deformation and gouge flow within the sheared zone might cause a similar effect. We assume that gouge and cataclastic zones, which have a thickness that primarily depends upon the amount of slip [Scholz, 1987; Power *et al.*, 1988], can reduce the wear of small asperities, while the relatively larger geometrical irregularities are selectively decapitated by fracturing and by interlocking mechanisms. However, such an assumption should be tested under much larger slip distances than attempted here.

## 5. Conclusions

Our experiments demonstrate that shearing of perfectly matching surfaces causes asperity smoothing at all measured scales, where asperity height decapitation is statistically correlated with the measured wavelength and with the displacement magnitude (equation (1) and Figure 4). Therefore, if an initial surface roughness is characterized by a power law (equation (2)) as function of the length [e.g., Power *et al.*, 1988; Renard *et al.*, 2006], then our results imply that the power will remain constant after slip but that the coefficient will decrease with increasing amount of slip (Figure 4). When the shear surfaces are not perfectly matched due to either previous shearing cycles, dilation, or wear layer generation within the fault aperture, the smaller-scale asperities might be less affected by interlocking deformation, and therefore, smoothing is expected to be less efficient at these scales.

### Acknowledgments

We thank Gil Cohen, Eran Sharon, Dorit Korngreen, Emily Brodsky, and Nir Badet. We thank Andrea Bistacchi and an anonymous reviewer for their critical review. This research was funded by Israel Science Foundation through grant 929/10.

The Editor thanks Andrea Bistacchi and an anonymous reviewer for their assistance in evaluating this paper.

### References

- Amitrano, D., and J. Schmittbuhl (2002), Fracture roughness and gouge distribution of a granite shear band, *J. Geophys. Res.*, *107*(B12), 1978–2012, doi:10.1029/2002JB001761.
- Archard, J. F. (1953), Contact and rubbing of flat surfaces, *J. Appl. Phys.*, *24*, 981–988.
- Barton, N. (1973), Review of a new shear-strength criterion for rock joints, *Engineer. Geol.*, *7*, 287–332.
- Bistacchi, A., W. A. Griffith, S. A. Smith, G. Di Toro, R. Jones, and S. Nielsen (2011), Fault roughness at seismogenic depths from LIDAR and photogrammetric analysis, *Pure Appl. Geophys.*, *168*, 2345–2363.
- Boneh, Y., A. Sagy, and Z. Reches (2013), Frictional strength and wear-rate of carbonate faults during high-velocity, steady-state sliding, *Earth Planet. Sci. Lett.*, *381*, 127–137.
- Bouchaud, E., G. Lapasset, and J. Planès (1990), Fractal dimension of fractured surfaces: A universal value?, *Europhys. Lett.*, *13*, 73–79.

- Brodsky, E. E., J. J. Gilchrist, A. Sagy, and C. Colletini (2011), Faults smooth gradually as a function of slip, *Earth Planet. Sci. Lett.*, *302*, 185–193.
- Brown, S. R., and C. H. Scholz (1985), Broad bandwidth study of the topography of natural rock surfaces, *J. Geophys. Res.*, *90*, 12,575–12,582.
- Candela, T., F. Renard, M. Bouchon, A. Brouste, D. Marsan, J. Schmittbuhl, and C. Voisin (2009), Characterization of fault roughness at various scales: Implications of three-dimensional high resolution topography measurements, *Pure Appl. Geophys.*, *166*, 1817–1851, doi:10.1007/s00024-009-0521-2.
- Chen, G., and H. Spetzler (1993), Topographic characteristics of laboratory induced shear fractures, *Pure Appl. Geophys.*, *140*, 123–135.
- Cowie, P. A., and C. H. Scholtz (1992), Displacement-length scaling relationship for faults: Data synthesis and discussion, *J. Struct. Geol.*, *14*, 1149–1156.
- Dieterich, J. H., and D. E. Smith (2009), Nonplanar faults: Mechanism of slip and off-fault damage, *Pure Appl. Geophys.*, *166*, 1799–1815.
- Dunham, E. M., D. Belanger, L. Cong, and J. E. Kozdon (2011), Earthquake ruptures with strongly rate-weakening friction and off-fault plasticity, Part 2: Nonplanar faults, *Bull. Seismol. Soc. Am.*, *101*(5), 2308–2322.
- Feder, J. (1988), *Fractals*, pp. 283, Plenum, New York.
- Goodman, R. E., and J. Dubois (1972), Duplication of dilatancy in analysis of jointed rock, *J. Soil Mech. Foundns Div.*, *98*(4), 399–422.
- Griffith, W. A., S. Nielsen, G. Di Toro, and S. A. Smith (2010), Rough faults, distributed weakening, and off-fault deformation, *J. Geophys. Res.*, *115*, B08409, doi:10.1029/2009JB006925.
- Muhuri, S. K., T. A. Dewers, T. E. Scott Jr., and Z. Reches (2003), Interseismic fault strengthening and earthquake-slip stability: Friction or cohesion?, *Geology*, *31*, 881–884.
- Ohanaka, M. (2004), A constitutive scaling law or shear rupture that is inherently scale dependent, and physical scaling of nucleation time to critical point, *Pure Appl. Geophys.*, *161*, 1915–1929.
- Parsons, T. (2008), Persistent earthquake clusters and gaps from slip on irregular faults, *Nat. Geosci.*, *1*(1), 59–63.
- Power, W. L., and T. E. Tullis (1989), The relationship between slickenside surfaces in fine-grained quartz and the seismic cycle, *J. Struct. Geol.*, *11*, 879–893, doi:10.1016/0191-8141(89)90105-3.
- Power, W. L., T. E. Tullis, and J. D. Weeks (1988), Roughness and wear during brittle faulting, *J. Geophys. Res.*, *93*(B12), 5268–15,278.
- Queener, C. A., T. C. Smith, and W. L. Mitchell (1965), Transient wear of machine parts, *Wear*, *8*, 391–400.
- Rangers, N. (1970), Influence of surface roughness on friction properties of rock planes, *ISRM, Proc.*, *1*, 1–19.
- Renard, F., C. Voisin, D. Marsan, and J. Schmittbuhl (2006), High resolution 3D laser scanner measurements of a strike-slip fault quantify its morphological anisotropy at all scales, *Geophys. Res. Lett.*, *33*, L04305, doi:10.1029/2005GL025038.
- Renard, F., K. Mair, and O. Gundersen (2012), Surface roughness evolution on experimentally simulated faults, *J. Struct. Geol.*, *45*, 101–112.
- Sagy, A., and E. E. Brodsky (2009), Constraints on faulting mechanism using 3D measurements of natural faults, in *Shear Physics at the Meso-scale in Earthquake and Landslide Mechanics*, edited by Y. Hatzor, J. Sulem, and I. Vardoulakis, pp. 145–158, CRC Press, Boca Raton, Fla.
- Sagy, A., E. E. Brodsky, and G. J. Axen (2007), Evolution of fault-surface roughness with slip, *Geology*, *3*, 283–286.
- Scholz, C. H. (1987), Wear and gouge formation in brittle faulting, *Geology*, *15*, 493–495.
- Scholz, C. H. (2002), *The mechanism of earthquakes and faulting*. ISBN 0-521-65223-5. 496 p.
- Segall, P., and D. D. Pollard (1983), Nucleation and growth of strike slip faults in "granite", *J. Geophys. Res.*, *88*(B1), 555–568.
- Wang, W. B., and C. H. Scholz (1994), Wear processes during frictional sliding of rock: A theoretical and experimental study, *J. Geophys. Res.*, *99*(B4), 6789–6799.